



Kashf Journal of Multidisciplinary Research

Vol: 02 - Issue 2 (2025)

P-ISSN: 3007-1992 E-ISSN: 3007-200X

https://kjmr.com.pk

CHEMICAL AND PHYSICAL FRONTIERS IN HIGH-TEMPERATURE SUPERCONDUCTIVITY

MD Alif Hossen Sany

School of Mechanical Engineering, Jiangsu University, Zhenjiang China.

Zeeshan Khan

Department of Physics, Abdul Wali Khan, University, Mardan.

Hanif Ullah

Department of Physics, Abdul Wali Khan, University, Mardan Alamgir Khan

Department of Physics, Abdul Wali Khan,

University, Mardan

Abdur Rahman

Department of Physics, Abdul Wali Khan,

University, Mardan

Muhammad Javed

Department of Physics, Abdul Wali Khan,

University, Mardan

*Corresponding author: <u>alamgirkhan03414946231@gmail.com</u>

Article Info



Abstract

High-temperature superconductivity remains a major frontier in condensed matter physics, offering potential breakthroughs in energy transmission, quantum computing, and advanced electronic applications. This review explores the chemical and physical principles underlying high-temperature emphasizing superconductors (HTS), their synthesis. characteristics, and electronic properties. The discovery of cup rate and ironbased superconductors has challenged conventional BCS theory, introducing novel mechanisms such as strong electron correlations and unconventional pairing symmetries. Advances in doping strategies, pressure-induced superconductivity, and interface engineering have significantly enhanced critical temperatures and performance. Recent experimental techniques, including angle-resolved photoemission spectroscopy (ARPES) and scanning tunneling microscopy (STM), provide deeper insights into HTS phase diagrams and their quantum states. Additionally, the role of chemical substitutions, lattice distortions, and electron-phonon interactions in modulating superconductivity is discussed. Challenges such as material instability, synthesis complexities, and the search for room-temperature superconductors remain key research directions. Emerging materials, including hydrogen-based and nickelate superconductors, suggest promising pathways for next-generation applications. By integrating theoretical models with experimental discoveries, this review highlights the fundamental and applied advancements in high-temperature superconductivity, paving the way for novel materials with enhanced superconducting properties. The interplay of chemistry and physics continues to drive innovations in this field, shaping the future of superconducting technologies.

@ 0

This article is an open access article distributed under the terms and conditions of the Creative Commons Attribution (CC BY) license

https://creativecommon s.org/licenses/by/4.0

Keywords:

Material Engineering, High-Temperature Superconductors (HTS), Electron Correlations.

Introduction

Superconductors provide magnetic flux field expulsion and zero resistance when electricity flows through them [1]. Moreover, superconducting materials have broad applications in many fields, such as grids that can transmit power without energy loss, ultrafast levitating trains that ride frictionless magnets instead of rails, and quantum computing devices that use superposition and quantum entanglement to perform computation [2]. As the most effective energy carrier, electricity is clean, versatile, and pervasive. However, power losses are produced when the electrical current flows in the coils and the magnetic field alternates in the core. For example, electric transformer losses in the current grid are substantial. Using eco-friendly superconducting materials to replace the current grid can enormously improve the efficiency of electric transmission. In modern technology, superconducting Al, Nb, and Ta are widely used in superconducting qubits for quantum computers for the preservation of quantum coherence[3]. However, the application of superconductors is far from real due to their low superconducting transition temperatures. Thus, pursuing materials that are superconducting under ambient conditions, i.e., room temperature and ambient pressure, is one of the major goals for physicists, chemists, and materials scientists. Superconductivity was first discovered by Ones in Hg with a critical temperature (Tc) of 4.2 K in 1911[4]. Ever since its discovery, it has stimulated significant interest in the research community to look for new superconductors with a higher transition temperature (Tc), new phenomena closely coupled with superconductivity, and new theories to understand the superconducting mechanism. Subsequently, researchers discovered many superconducting families of materials in different elements, alloys, intermetallic compounds, and oxides in various forms, either bulk or thin film. shows the timeline of several major groups of superconductors and highlights the most representative ones in them. Here in the first section, we will briefly introduce some representative types of superconductors in the order of time. Note that this review is not an exhaustive introduction to superconductors, so we will only discuss several representative ones that are superconducting at the highest temperatures or discovered earliest. In the 1950s, the Bardeen-Cooper-Schrieffer theory (BCS)11 successfully explained the mechanism of phonon mediated superconductivity. This well-known superconductivity mechanism was established by John Bardeen, Leon Cooper, and John Robert Schrieffer. The fundamental picture of the BCS theory is that electron-phonon coupling induces a superconducting state by pairing up electrons with opposite spins and crystal momenta (that is, total momentum zero). The Cooper pair, as part of a highly correlated state, is free to move through the lattice, in contrast to a localized electron pair. Moreover, in BCS theory, the pairing of electrons occurs in momentum space, a space defined reciprocally to real space, and the Cooper pair cannot be described locally. The BCS theory fails to provide definite theoretical predictions for new superconductors. Therefore, the synthesis of novel superconductors is still plagued by mystery and challenges. In addition, the superconductors whose superconducting mechanisms can be explained by BCS theory are normally called BCS superconductors (SCs) or conventional SCs (CSCs), while others are called unconventional SCs (UCSCs). From a chemical viewpoint, the BCS theory can be simplified, but may not be rigorous enough, into the following picture: when the material is superconducting, two moving electrons with opposite wave vectors and spins in a lattice attract each other and form Cooper pair through phonon mediation where the phonon is the vibration of the lattice. Cooper pairs move in the lattice as a condensate without resistance. To break one Cooper pair, it requires the energy of 2Δ , in which Δ is the superconducting energy gap [5]. This indicates that the energy from the oscillation of atoms is too weak to break Cooper pairs, and thus, zero resistance can persist. The relation between Δ and Tc is given by this equation: $2\Delta(0) =$ 3.52kBTc, where kB is the Boltzmann constant and $\Delta(0)$ indicates the theoretical superconducting energy gap at 0 K. In 2014, the world's longest high-temperature superconducting (HTS) cable was integrated into the Essen power grid (Germany), replacing a 110 kV high-voltage cable with a more efficient 10 kV HTS cable, reducing space and energy losses [6]. The system also includes a fault-current limiter that prevents damage by switching to a resistive state under high current loads. Various companies have developed faultcurrent limiters for commercial use. HTS materials are also applied in electromechanical machines such as motors and generators, where they reduce energy losses and enable compact, high-performance designs. For

example, American Superconductor developed a 36.5 MW HTS ship propulsion engine that is significantly lighter and smaller than conventional engines. HTS materials are also used in energy storage systems, including superconducting magnetic energy storage (SMES) and flywheel energy storage (FES) devices, improving efficiency and compactness [7]. Superconducting magnetic levitation (SC Maglev) trains, such as those developed by JR Central, utilize HTS coils to achieve high-speed, frictionless travel. In 2015, a SC Maglev train set a world record of 603 km/h, with commercial operations planned for 2027 between Tokyo and Nagoya. HTS technology also finds applications in electronics, particularly in wireless communication, where HTS filters enhance signal range in cell phone base stations. Other applications include High-Q resonators in particle accelerators and SOUIDs (Superconducting Quantum Interference Devices), which detect tiny magnetic fields for medical diagnostics, material testing, and scientific research. SQUIDs can measure magnetic fields from human heart and brain activity with high precision. High-temperature superconductors (HTS) face several challenges, including unclear superconducting mechanisms, material instability, and the need for extreme conditions like high pressure. Their limited ability to sustain superconductivity under strong magnetic fields and high currents restricts practical applications in power grids and electronics. Additionally, high costs and cooling requirements hinder widespread adoption. This review aims to explore the chemical and physical principles of HTS, investigate unconventional superconducting mechanisms, and highlight advancements in material engineering and experimental techniques. By bridging the gap between theory and application, it seeks to provide insights into overcoming current limitations and advancing HTS research for future technological applications.

2 Common HTS materials (cup rate, iron based superconductors, etc.)

Superconductivity is a phenomenon of exactly zero electrical resistance and expulsion of magnetic fields occurring in certain materials when cooled below a characteristic critical temperature. It is a macroscopic quantum phenomenon. Its special physical properties have attracted the attention of many physicists and electric engineers, since it was discovered by Ones in 1911. Superconductivity with its flow of electric current without friction amounts to the realization of the old human dream of a perpetuum mobile. The ratio of resistance between the normal-conducting and the superconducting ("SC") state has been tested to exceed 1014, i.e., it is at least as large as between a usual insulator and silver as the best normal-conducting material 1 . As the progress of cooling technique gave access to lower and lower temperatures, superconductivity established as common low-temperature instability of most, possibly all metallic systems (see Fig. 1). However, even though many types of superconductors were discovered for many years, the critical temperature was below 20K, thus, the uses of superconductor's required cooling using liquid helium. After Nb3Ge (Tc = 23.2 K) was discovered in 1973, the critical temperature did not increase by even 1K for more than 10 years. Through the 1970s and 1980s, several types of experiments and theoretical discussions were carried out to discover "high-temperature superconductivity". It is important to remember what happened in this prehistoric era. Twenty seven years have passed since the first sample of high temperature superconductivity was discovered in La2- xBaxCuO4 in 1986. . However, for practical application of superconductors we need superconductors with higher critical temperature and cup rate is best for this. A superconductor can be distinguished by following two properties: (i) Vanishing of electric resistivity below a critical temperature (Tc). (ii) Expulsion of external magnetic field below a critical field (Hc). In cup rate superconductor electric conduction arises from the pairing of charge carriers into copper pairs [8]. Superconductivity is believed to be a universal phenomenon, and is a collective state existing in electron population of a material. From superconducting cosmic strings created as topological defects in the early universe [9].or proton superconducting cores in neutron stars4 to color superconductivity in quark matter.[10].

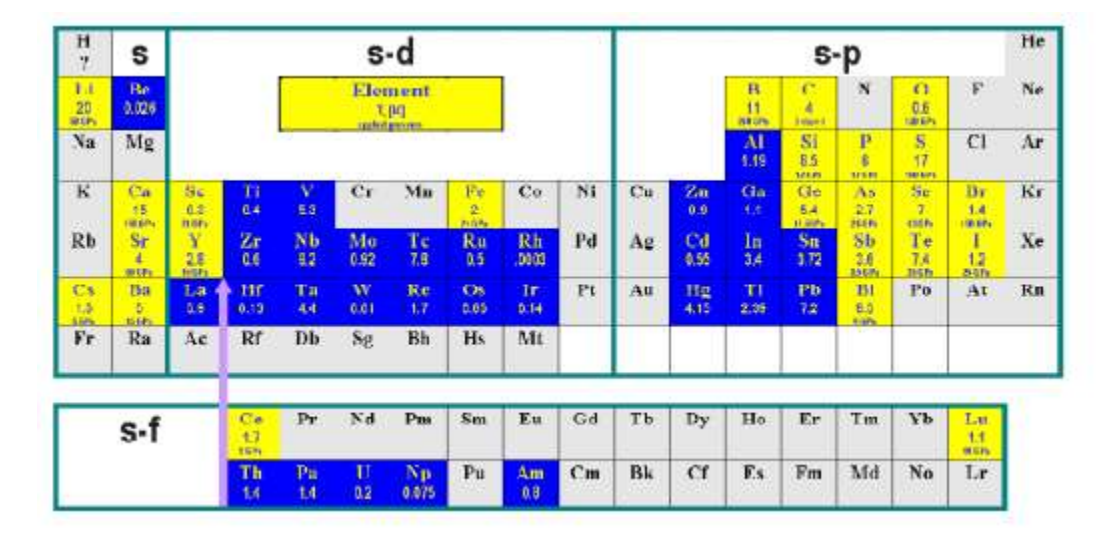


Figure 1: Periodic table with the distribution and Tc [K] of the chemical elements for which superconductivity has been observed with or without application of pressure [11].

Cuprite Superconductors:

In more than 24 years elapsed from the discovery of high Tc superconductivity in copper oxides, a huge number of experimental and theoretical investigations of the physical properties of these materials have been done. The high temperature superconductivity of cup rates was discovered in 1986, when the highest superconducting transition temperature (i.e., critical temperature) characteristic of conventional superconductors (Tc =23.2 K in Nb3 Ge) was substantially exceeded and a superconducting transition temperature Tc =30K was achieved in the ceramic La2- xBaxCuO4-δ. The situation including the high Tc cup rate superconductors is illustrated in Fig. 2(b). Within a year after this discovery, the record value of Tc exceeded 90 K (YBa2Cu3O7- δ ceramic). The further search for and creation of new superconducting materials led to Tc=138K (Tl-doped HgBa2Ca2Cu3O8- δ compound) in 1994 and raised the question of room-temperature superconductivity. In spite of all these efforts, the mechanism of this new kind of superconductivity has not been clarified yet; it still remains one of the most enigmatic problems of the solidstate physics. The description of their normal state properties has turned out to represent an even bigger challenge to solid-state physics theory. The difficulty of this problem is due to the complicated properties, including complicated crystalline structures of materials displaying high Tc, to the presence of a strong anisotropy, to the existence of non-adiabatic effects, to strong electronic correlations, and to a strong electron—phonon interaction In these complicated materials, several phase transitions (structural, magnetic, superconductor, etc.) occur, and mixed states are allowed, for instance coexistence of superconductivity and ferromagnetism or vitreous spin state. The key structural element of layered quasi-two-dimensional cup rates is a (CuO2) plane (one or several in a unit cell); they differ from conventional superconductors not only in high values of Tc but also in a set of physical properties that cannot be described by the classical Bardeen-Cooper–Schrieffer (BCS) scheme. In cup rates, charge carriers appear due to the doping of the CuO2 planes of a parent antiferromagnetic insulator upon nonsolvent atomic substitution or the creation of oxygen vacancies in charge reservoirs outside the conducting planes. The distance between equivalent CuO2 planes in neighboring unit cells is large compared to the in-plane distance between neighboring copper atoms, which results in a strong conductivity anisotropy at temperatures above Tc and the two-dimensional coherence of the superconducting state at temperatures below Tc. The highlighting feature of this type of superconductors that is more attractive for application point of view is the very high upper critical field. Before discussing the characteristics and application of cup rate family we will discuss about some basic properties of superconductors. Because these properties are also present in cup rate superconductors.

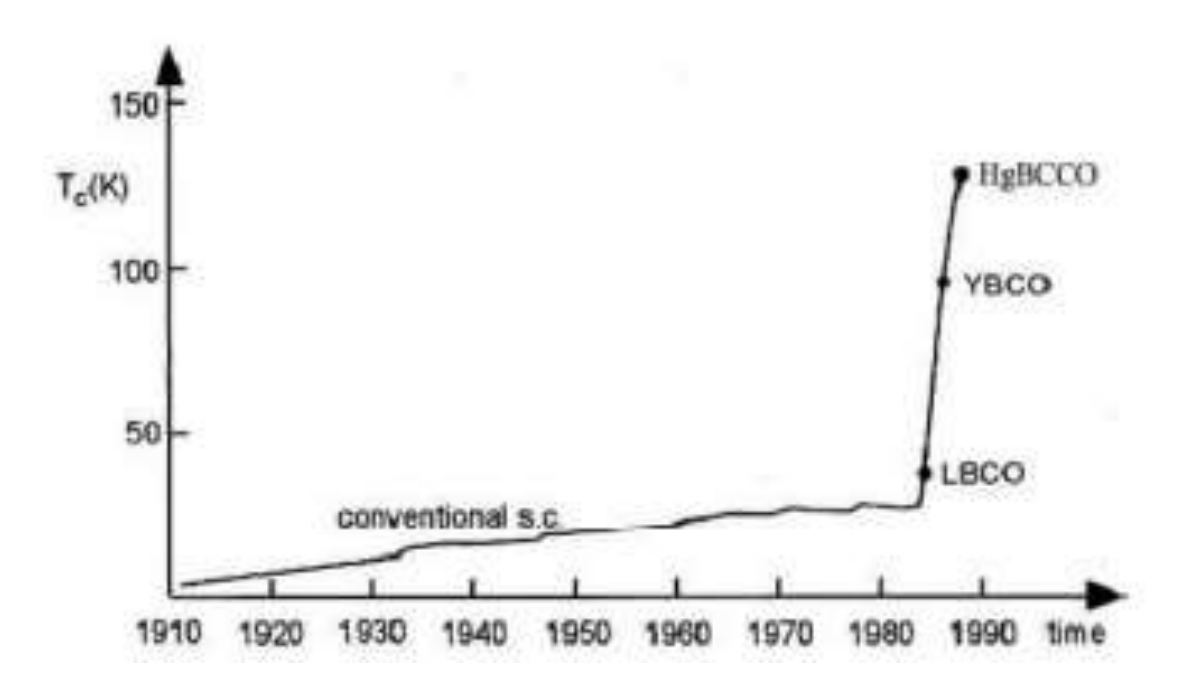


Figure 2: High-Tc cup rate superconductors discovered by Bednorz and Mueller in 1986. For La2-xBaxCuO4 a Tc ≈ 35 K, for YBa2Cu3O7-δ a Tc = 92K, and for HgBa2Ca2Cu3O8+δ a Tc = 133K was observed, for example.

Common Characteristics of Superconductors

After invention of high-temperature superconductivity in cup rate based material many characteristics of these material has been invented. Among all of these characteristics some are common in all cup rate family such as electronic structure etc. In this section characteristics will be discussed. The specific will be discussed in later section

Compounds	Crystal Structure	Size of elementary cell, A	T_{c} K
La _{2-x} Sr _x CuO ₄ (La=Sr-214)	Tetragonal	a = b = 3.78; $c = 13.2$	37.5
YBa ₂ Cu ₃ O ₇ (123)	Orthorhombic	a= 3.82; b = 3.88; c = 11.7	90
$BiSr_2CaCu_2O_8$ (Bi -2212)	Tetragonal	a=b=5.4; c=30.89	95
T IBa ₂ Ca ₂ Cu ₃ O ₉ (T1-1223)	Tetragonal	a=b=3.85; c=15.9	120
T I ₂ Ba ₂ CuO ₆ (T I - 2201)	Orthorhombic	a=5.468; b=5.473; c=23.24	90
T I ₂ Ba ₂ CaCu ₂ O ₈ (T1 - 2212)	Tetragonal	a=b=3.86; c=29.3	112
T l ₂ Ba ₂ Ca ₂ Cu ₃ O ₁₀ (T1-2223)	Tetragonal	a=b=3.85; c=35.9	125
HgBa ₂ Ca ₂ Cu ₃ O ₈ (Hg -1223)	Tetragonal	a=b=3.85; c=15.9	133
HgBa ₂ Ca ₃ Cu ₄ O ₁₀ (Hg - 1234)	Tetragonal	a=b=3.85; c=19	127

Table 1. Crystal structure and elementary cell of some cup rates

Application of Cup rate Based Superconductors

Due to the unique properties of high temperature superconducting materials, their applications are becoming attractive continuously with the improvement in properties of superconductors. The search for applications has always been a driving force for superconductor materials science. Right from the discovery, it had been envisioned that superconducting (SC) coils with high persistent current might be used to produce strong magnetic field. In the last ten years, many applications of high temperature superconductors have been developed. In this section some typical applications of cup rate based superconductors will be discussed.

Superconducting Bulk

Superconducting bulk YBCO is grown using half-metal materials at a high temperature of nearly 1000oC, followed by a very slow cooling. The special feature of the bulk is that the introduction of pinning centers is easily carried out by controlling the density of fine Y2BaCuO5 particles as pinning centers in the bulk. The most distinguishing characteristic is that it is possible to trap a strong magnetic field of 2 to 3T, even at liquid nitrogen temperature. This value is much higher than the magnetic field of an ordinary permanent magnet. Superconducting bulk has been applied as a bearing system that is used to store electricity in a flywheel system, as shown in Fig. 18. The capacity of this system is about 10 KW/h and it has operated safely for many months. The second application is a magnetic separation system for the water cleaning made by Hitachi, Ltd. The impurity particles in water join magnetic particles, and they are removed from the filter by the strong magnetic field of the bulk. The operation can be continuous and results have been impressive [12]. The effect of boron excess in the structure and superconducting properties of NbB2 is reported. Rietveld refinements of the x-ray diffraction patterns indicate that boron excess induces significant changes in the Nb-B bond length, increasing the c-axis. In contrast, the B-B bond length remains essentially constant. Magnetization behavior was studied in the temperature range from 2 to 15 K. We found that for (B/Nb)exp 2.20(2) of boron excess samples display superconductivity with a maximum TC of about 9.8 K at (B/Nb)exp = 2.34(1). High pressure measurements in samples with two different boron contents reveal that TC decreases at different ratios, dTC/dP. Superconducting parameters were determined, indicating that NbB2+x is a type II superconductor. Theoretical studies related to band structure of NbB2 by Shein and Ivanovskii[13]. show an enhancement of the covalent interactions between boron and Nb planes (due to hybridization of the B 2p– Nb d states), which in turn changes the density of states at the Fermi level N(EF); this fact must also be valid for the non-stoichiometric NbB2+x compound. Then, N(EF) will change with the atomic ratio B/Nb, giving a peak in the density of states at the Fermi level, TC thus reaching a maximum value [14]. In this context it will be interesting to probe theoretical predictions by performing systematic experimental studies in nonstoichiometric NbB2, in order to understand the role of excess boron in structural and superconducting properties of the compound. In this work we will show the importance of defects in the electronic properties of NbB2. We report that in NbB2+x, careful synthesizing procedures allow us to increase the transition temperature to about 9.8 K, for (B/Nb)exp in the range 2.32(1)-2.34[15]. We analyse the changes of the lattice parameters due to boron excess, and the superconducting state. Additionally, we compared this behavior with our high pressure experiments performed using a diamond anvil cell. Figure 1 shows the powder x-ray diffraction patterns of NbB2+x samples with nominal compositions B/Nb from 2.0 to 2.6. [16]. These correspond to the NbB2 common structure (No 75- 1048 of the International Centre for Diffraction Data ICDD). The impurities observed are faint features of Nb5B6 (ICDD No 42-1040), B2O3 (ICDD No 76-1655) and Nb2O5 (ICDD No 80-2493). Diffraction patterns were fitted using Rietveld analysis, with the hexagonal AlB2 structure model and space group P6/mmm (No 191). The analysis shows that the majority phase is NbB2+x > 90%. Figure 2 shows an example of the Rietveld analysis for the composition with B/Nb = 2.0. Structural analysis extracted from Rietveld refining considering NbB2+x structure, see figure 3, indicates the occupancy factor for niobium and boron as a function of boron excess [17]. However, the real niobium occupation factor is included in table 1 using the Nb1-xB2 stoichiometry. This must be compared to the boron nominal starting compositions, B/Nb. It seems that for compositions below B/Nb 2.3 both are similar. As the nominal composition increases from B/Nb = 2.35 to 2.6 Rietveld refining determines the real composition, given $(B/Nb)\exp = 2.30(1)-2.34(2)$ with respect to the B/Nb values. The structural parameter data are listed in table 1.

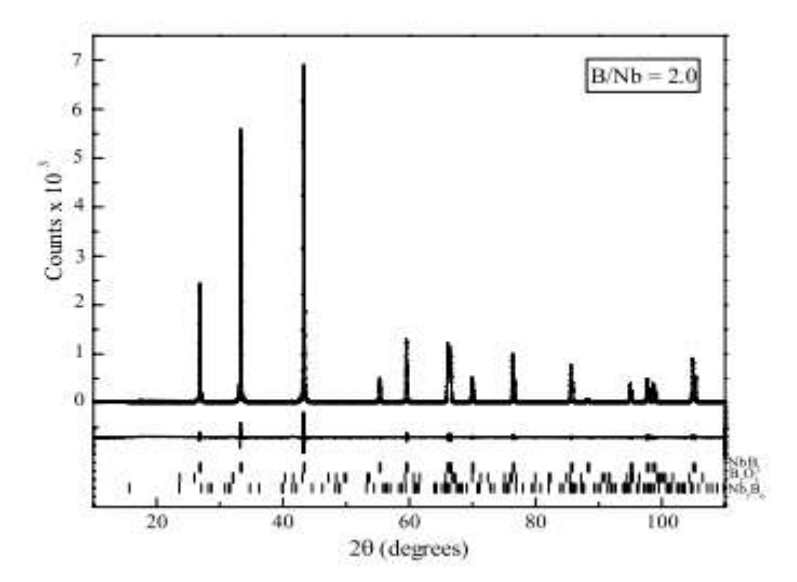


Figure 3: Example of Rietveld refinement for the NbB2 sample. X-ray experimental diagram (dots), and calculated pattern (continuous curve), difference (middle curve) and calculated peak positions (bottom). A superconducting powder was separated with a magnet making use of the Meissner effect in liquid nitrogen[18].

A single crystal 16X 70X 120 pm was selected and mounted on a Picker diffractometer with graphitemonochromatized Cu Ka radiation. The body-centered tetragonal cell derived from the interpretation of the powder pattern was confirmed. The cell parameters a 3.814 A. and c 30.52 A obtained on this crystal are quite poor because the crystals are buckled due to their small thickness. Due to this buckling, the normal to the atomic planes changes direction with the point on the crystal. Consequently, the reciprocal lattice nodes are spread out on circular arcs parallel to [001] for hk0 reflections and on a spherical cap for 001 reflections. This angular spreading of about 1' ruled out the use of Mo radiation because of reflection overlap; therefore, we used the Cu radiation [19]. Even with this longer x-ray wavelength reflection overlap was not completely eliminated, and also, part of the diffracted intensity did not reach the counter for large Bragg angles. In spite of these experimental difficulties, crude diffraction intensities could be measured. A survey of reflection intensities symmetry-related in Laue group 4/mmm but not in Laue group 4/m indicated Laue group 4/mmm. The reflection profiles were displayed on a screen for comparison. Intensity measurements up to 120' Bragg angle followed by averaging of the symmetry-related intensities after absorption correction by Gaussian integration gave 143 unique reflections, 111 of which were observed. Although the tetragonal diffraction aspect E—- combined with Laue class 4/mmm allows the space group E422, E4mm, E4m2, E42m, and E4/mmm, the very short a and b repeats force the fractional coordinates for the metal atoms to be 0 and —, ' for an ordered tetragonal structure in all these space groups[20]. As the diffraction intensities do not contain a class of reflections so weak that it could be due to oxygen only, it follows that the metal contribution, which dominates the diffraction intensities for all classes of reflections, can be phased in space groups E4mm or E4/mmm. The reflections being phased by the metals, the oxygens should be visible on difference-Fourier maps and lower symmetry should be indicated by split peaks on the difference maps or by fractional refined occupancies. The space group 14/mrnm, which is centrosymmetric, is more likely for a high-temperature oxide[21].

The Phase Diagram of High-Pressure Oxygenized Compounds

In parallel with the quantum phase diagrams of conventional cup rates, the dependence of Tc on p can also be shown for LCO-O- and YBCO-type for HPO compounds in a second one (Figure 4), with single points for the former and multiple points for certain of the latter compounds. Instead of being suppressed by "over

doping", superconductivity is maintained or even enhanced upon achieving remarkably high O stoichiometries and corresponding p values; up to p=0.6 in Sr2CuO3 (Tc = 95 K) and p=1.0 in CuBa2YCu2O8 (Tc = 91 K). These data were compiled from the literature (Table 1), with the graph and table compiled from only a fraction of the reports. Doping was performed by both O addition and aliovalent cation substitution [22]. The reliability of the O analysis methods that validate the O stoichiometry is discussed in the next section.

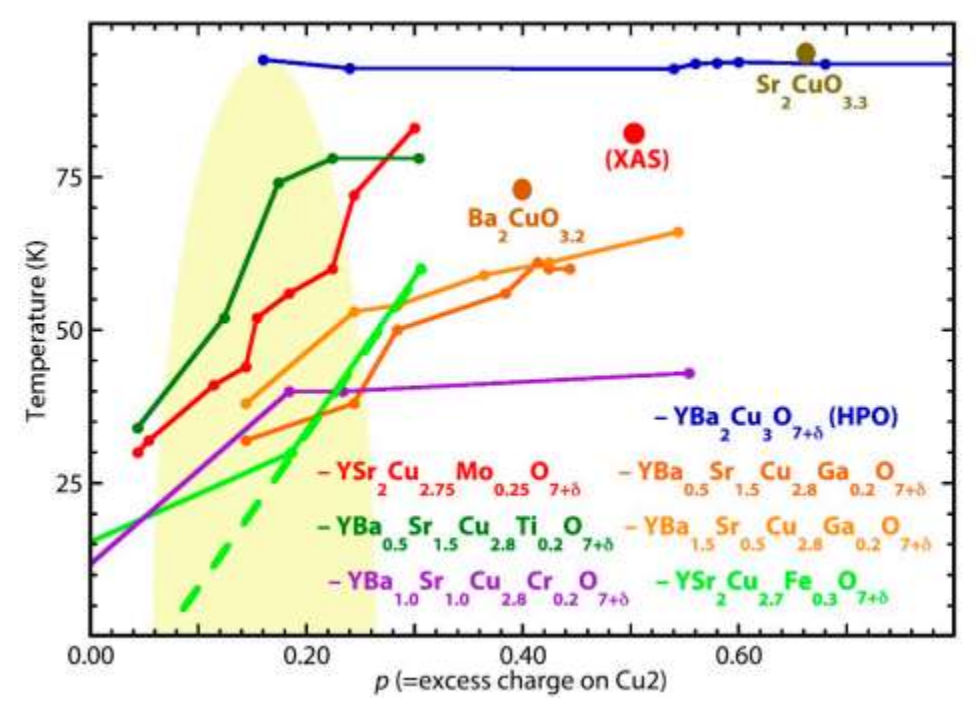


Figure 4: The quantum phase diagram for the listed HPO compounds.

The CuBa2YCu2O7 $\pm\delta$ (YBCO)-type was selected because its multiple O stoichiometries display the transit of their superconductivity through the "dome" with no decrease in their transition temperatures. The point labeled "XAS" is the experimentally determined charge on the Cu in the CuO2 plane for YSCO-Mo, demonstrating that the excess charge calculated from the stoichiometry and assumption of Mo(VI) is a lower bound [23]. Only single points are available for Sr2CuO3+ δ and Ba2CuO3+ δ , although Sr2CuO3+ δ has multiple superconducting phases with a range of transition temperatures associated with subtle crystallographic differences that may also originate in small differences in O stoichiometry[24] .

High-Pressure Oxygen Synthesis of Hyper Stoichiometric Superconducting Cup rates One often-overlooked influential factor for Tc, and especially for its experimental de-termination, is sample preparation. Especially, pressure is recognized to strongly influence bonding and crystal structure; many investigated phases are metastable at ambient pressure. Crucial for our discussion, however, is how pressure affects the positions of the excess oxygen within superconducting curates and, specifically, whether this position depends on the synthetic approach. Bond compression is known to affect the shape of the potential well for apical oxygen [25]. which is known to influence Tc. It is, therefore, useful to discuss the synthesis routes for HPO cup rates. The synthesis of highly oxygenated cup rates can, at most, include three different types of steps (Figure 5): • Ambient-pressure (AP) synthesis; • Low-pressure oxygenation (LPO) steps; • High-pressure oxygenation (HPO) treatment [26]. The most used ambient pressure (AP) synthesis method is conventional solid-state synthesis, in which primary precursors, often primary metal oxides or carbonates, are ground together and then repeatedly heated (annealed) with intermediate grinding. At high temperatures (usually 700–1200 °C), a solid-state rearrangement of atoms is mediated by enhanced diffusion. Variants of the solid-state method are the nitrate route [27], and sol-gel route [28], in which the primary precursors are initially mixed by dissolution, followed by drying and annealing with intermediate grinding. Low-pressure oxygenation (LPO) methods are taken to include the use of O2 atmosphere under ambient pressure synthesis [29]. but also

pressurized treatments in gas phase, e.g., in an autoclave [30],[31], at pressures up to ca. 25 MPa. Liquid-phase oxidation by NaOBr-solution stirring has also been described [32]. High-pressure oxygenation (HPO) is performed under extreme pressure of 1 GPa or higher, using a solid oxygen source. Described in Figure 6, the sample size is limited to the size of the equipment in question; this is, generally, fractions of a gram. Pressure is amplified and conveyed to the sample via WC anvils of varying geometry. Most common is the cubic anvil assembly. Nesting an octahedral anvil assembly within the cubic assembly creates the Walker-type multi-anvil module, which is used for ultra-high-pressure experiments up to ca. 25 GPa.

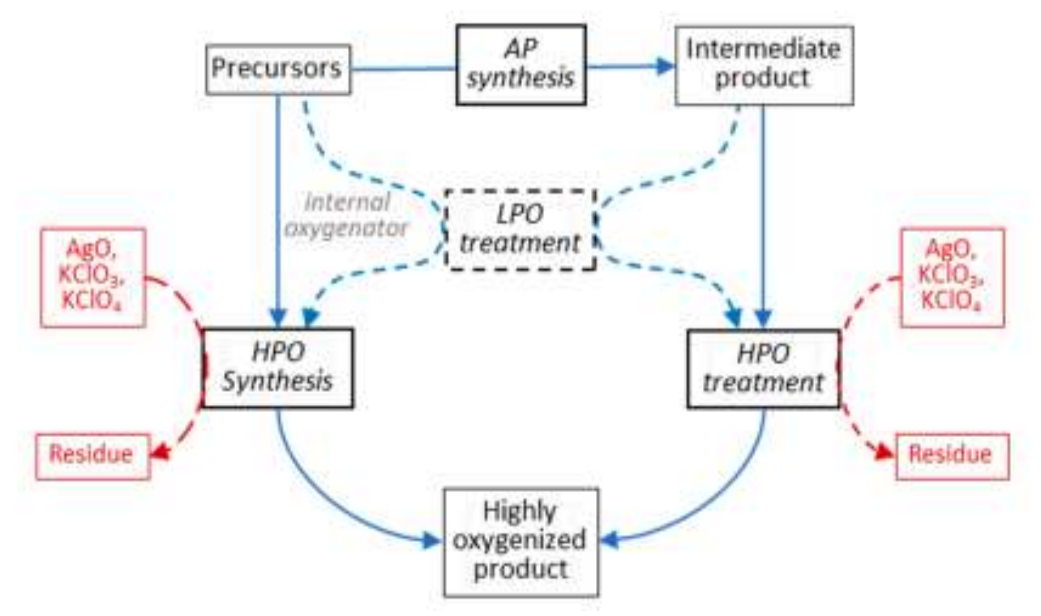


Figure 5. Flowchart of possible HP synthesis routes for strongly oxygenated cup rates.

In HPO synthesis, the final product is formed under pressure by reacting precursors together, where oxygen is provided by either an internal or external oxidizer. In HPO treatment, the ready-made product is oxygenated by an external oxidizer. In either case, intermediate LPO treatment can be used to boost the final oxygen content [33].

2D High-Tc Superconductors

Fe-Based high-Tc superconductors (HTS) have been a hot topic to study since the discovery in 2008 [34]. In the early time, quasi-2D thin films were detected to be superconducting with Tc just above the exceeding McMillan limit (40 K), which are considered to be HTS. The high-Tc superconductivity of these types of Fe-based superconductors have been explained by the strong spin fluctuations, which is caused by repulsive Interbrand interactions between the hole-like bands around the Γ and the electron bands around M[35]. In the last decade, monolayer FeSe have become a hot topic with the advanced MBE technique, which has a simple tetragonal PbO structure consisting the layered atomic stacking of Fe and Se atoms along the c-axis[36]. (shown in Figure 5a,d). Song et al. first used MBE to grow pristine FeSe films on graphitized SiC with a Tc lower than 10 K in 2011[37]. Further on, the superconductivity of monolayer FeSe grown on SrTiO3 (STO) undergoes an order of magnitude Tc enhancement up to 77 K, in 2012[38]. Since then, 2D Fe-based superconductors have been studied widely with its unique ultrahigh Tc, especially one-unit-cell FeSe/STO (1UC FeSe/STO). As shown in Figure 5b,c, the Tc of the monolayer FeSe/STO grown by MBE is evidenced to be about 53, 65, even up to 109 K, which are supported by in situ four-point probe transport [39]. To further investigate the underlying physics of the superconductivity enhancement in 1UC FeSe/STO system, three main modulation methods are applied: thickness variation, charge doping, and substrate modulation.

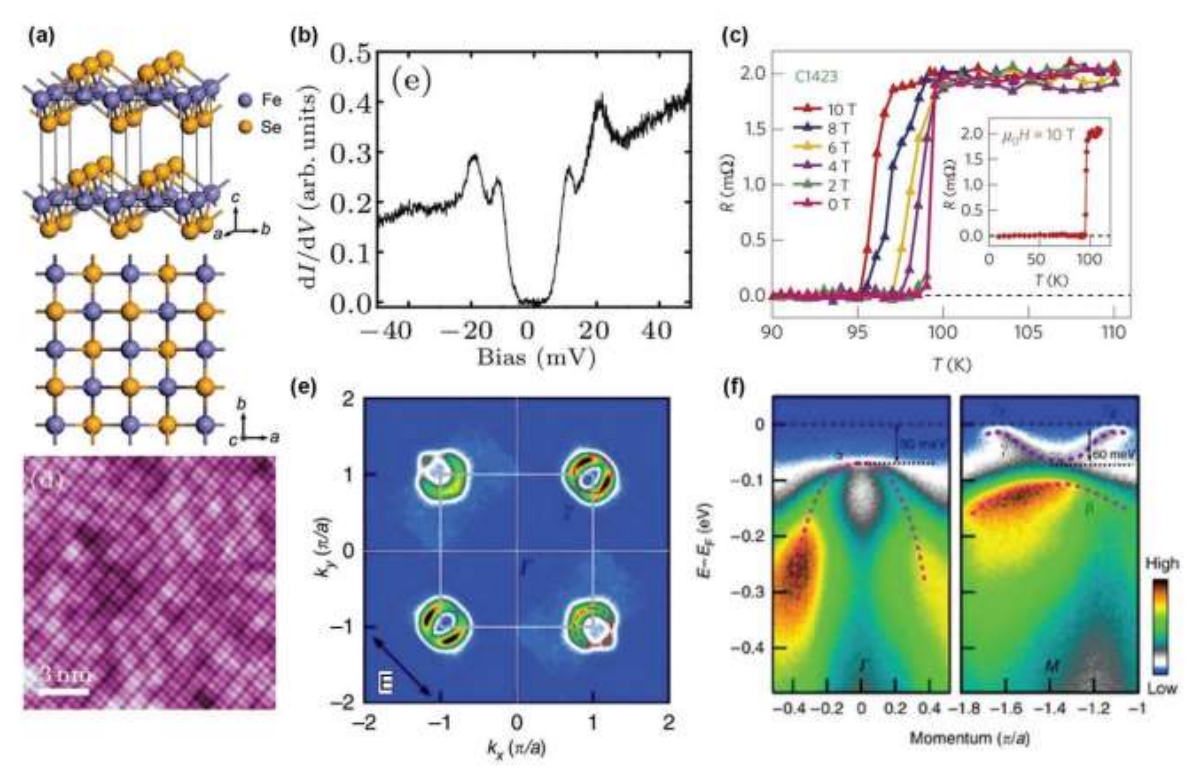


Figure 6: Characterization of 1 UC FeSe/STO.

a) Schematic drawing of β -FeSe lattice structure. b) STS on 1UC FeSe/STO showing the superconducting gap with four pronounced coherence peaks appear at ± 20.1 and ± 9 mV, respectively. c) Temperature dependence of the resistance obtained from a linear fit to the I–V curves, showing the ultrahigh Tc above 100 K. d) Atomically resolved STM topography (12.8 nm \times 12.8 nm). e) Fermi surface mapping of 1UC FeSe/STO measured at 20 K by APRES, which consists only of the electron-like Fermi-surface sheet (γ) around BZ corner M (π , π). f) Band structure along the cuts across the BZ Γ point (left) and M point (right), revealing a hole-like band (pink dashed line) and an electron-like band (purple dashed line). a) Reproduced with permission.[4] Copyright 2008, National Academy of Sciences. b,d) Reproduced with permission[38]. Copyright 2012, Chinese Physical Society and IOP Publishing Ltd. c) Reproduced with permission[39]. Copyright 2014, Springer Nature. e,f) Reproduced with permission [40]. Copyright 2012, Springer Nature.

MAGNETIZATION OF BULKS AND STACKS

In the fundamental studies of HTS modeling, the magnetization pattern of a HTS bulk or strip can be well modelled by H-formulation and the results are in good agreement with analytical solutions. In [41], the magnetization curves of an HTS bulk in the presence of different amplitudes [42], and frequencies of magnetic field were simulated in 2D. In [43] Zhang and Coombs used the 3D H-formulation to model a single HTS bulk and a bulk array, and showed that HTS bulk arrays can create a highly uniform magnetic field profile in a reasonably large domain. In [44], Zhang et al examined the pulse magnetization of an HTS bulk and studied the distribution of trapped field using the H-formulation. In [45] Kapolka et al studied different magnetization behaviors of HTS rectangular bulks and stacks in the presence of inclined fields using different 3D models, including the H-formulation. In [46] Ainslie et al performed a pulsed field magnetization (PFM) experiment for two c-axis oriented, single grain GdBCO and YBCO bulk superconductors, and used the 3D H-formulation model to investigate the effects of inhomogeneities on the trapped field and maximum temperature increase of the samples. In[47] a novel arrangement of the HTS bulk with magnetizing coils and iron yoke to trap high field was experimentally tested, and a 2D axisymmetric H-formulation model was used to qualitatively reproduce and monitor the magnetization process from the thermal and electromagnetic points of view. In [89], Ainslie and Fuji Shiro presented an overview of the modeling of HTS bulk magnetization, and proved that both the 3D and 2D axisymmetric H-

formulation models are viable tools for various conditions of HTS bulk research. In [48] Page et al carried out the experiment of pulsed magnetization for HTS stacks using multiple pulses with different temperatures, and used the 2D H-formulation and the real thickness of each layer in the HTS stack to accurately model the process of eddy current and heating effects. In [49] Baskys et al simulated trapped magnetic fields and critical current density of HTS stacked tapes with angular transversal field. In [50]Zou et al studied the influence of the n index and magnetic field constant B0 value in the Kim's model on the field trapped in HTS bulks by means of pulsed field magnetization. An example of an HTS bulk coupling cooling boundary and thermal insulation in the presence of pulsed magnetic field is presented in Figure 7, which shows the modeling scheme and the domains and the boundary conditions (Figure 7)the temporal evolution of the applied field pulse (Figure 3(b)) and some results at selected instants of the pulse (Figure 7)). In the last plot, the influence of the index n on the results for the current density distribution is clearly visible, as are the different results obtained with a purely electromagnetic model (on the left) and a coupled electromagnetic-thermal model (on the right). The same authors investigated an HTS stack magnetized using pulsed field magnetization by controlling the current of external coils based on H-formulation. Later, Zou et al performed experiments on HTS stack magnetization to validate the electromagnetic-thermal coupled 2D H-formulation model, and the results indicated that using suitable magnetization sequences could efficiently improve the trapped field.

LARGE-SCALE HTS APPLICATIONS

The H-formulation can be used to simulate the superconducting parts of large-scale HTS applications, in particular to investigate their electromagnetic performance (e.g. loss analysis) and to study the effect of screening currents. Shen et al used the H-formulation FEM model to develop superconducting magnets using a Halbach array configuration for transportable medical imaging device called Lorentz Force Electrical Impedance Tomography (LFEIT) and then they used optimization methods to further improve the uniformity of the superconducting magnet. As shown in Figure 4, Shen et al also incorporated the superconducting magnetic properties into the LFEIT system to simulate the magneto-acoustic signal from different biological samples. Xia et al evaluated the electromagnetic performance and calculated the AC losses of a highfield superconducting magnet using the H-formulation with anisotropic bulk homogenization model, with the purpose of getting insights for the superconducting prototype coils of the National High Magnetic Field Laboratory 32 Tesla all superconducting magnet. The H-formulation can be a useful tool for modeling superconducting fault current limiters. A 10 kV resistive type HTS fault current limiter was investigated by means of experiments and H-formulation calculations. In [101], Jia et al performed a loss and magnetic field analysis of a saturated iron-core superconducting fault current limiter (SISFLC). In addition to the spatial distribution of the AC losses, they studied the relationship between the AC component of the current and the AC losses. Shen et al investigated the details of the power dissipation of a threephase 35 kV/90 MVA SISFCL. The losses were estimated to be up to the kW level and potentially even higher, depending on the amplitude of the used DC bias current. Wang et al modelled a hybrid HTS magnet with around 7000 turns using the homogeneous bulk approximation. Such magnet was proposed to be applied in a superconducting magnetic energy storage (SMES) system. Using the same homogeneous bulk approximation, Song et Al simulated an HTS three-phase 1 MVA transformer, and compared the loss results with those previously obtained with the minimum magnetic energy variation (MMEV) model, finding a reasonably good agreement. Several studies have been reported on the modeling of HTS motor or generator applications based on the H-formulation. Hu et al used a 3D model to simulate all-superconducting synchronous electric machines, and they performed the analysis on the magnetic field around the HTS coils and proposed a method to reduce the total AC losses. Zhang et al simulated the HTS racetrack armature windings for largescale HTS machines and studied their magnetization and transport current AC losses. For HTS generators, Quéval et al combined the power grid analysis and the loss study of a 10 MW class HTS wind turbine generator. Li et al modelled the armature structures of a fully HTS synchronous generators with loss and electromagnetic analysis. Brambilla et al developed a hybrid A-H formulation to investigate the electromagnetic behavior of HTS electrical machines. The idea behind this approach was the separation of the model of an electrical machine in two parts, where the magnetic field is calculated with the most appropriate formulation: the H-

formulation in the part containing the superconductors and the A-formulation in the part containing conventional conductors (and possibly permanent magnets). The work focused on determining and applying the continuity conditions on the boundary separating the two regions.

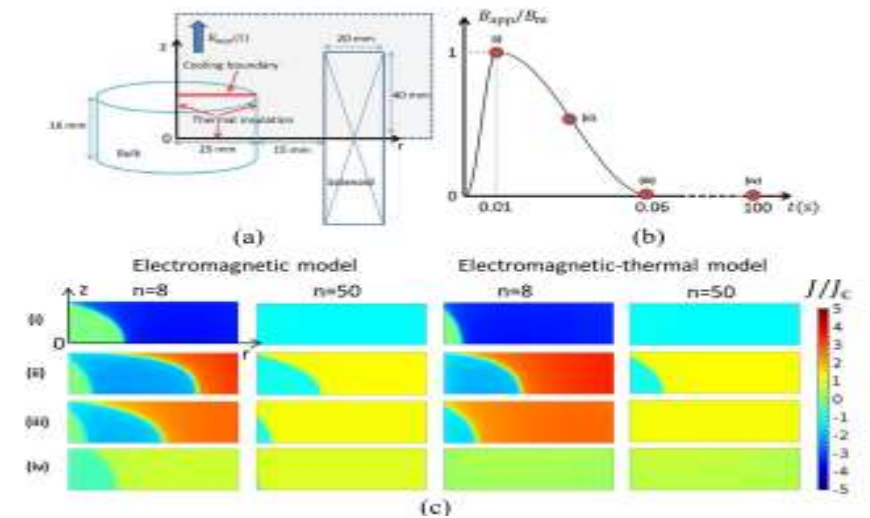


FIGURE 7 (a):An HTS bulk magnetized by pulsed field magnetization (PFM) with a solenoid using H-formulation, the upper boundary of HTS bulk was set as a cooling boundary with a given heat flux, and the other 3 boundaries of the HTS bulk are thermally insulated, (b) The applied magnetic field (normalized to its maximum value), 4 points are selected for analysis: (i) 0.01s, (ii) 0.035s, (iii) 0.06s, (iv) 100s, (c) the normalized current density distributions J/Jc at selected times, with different values of n, with figure source: [51].

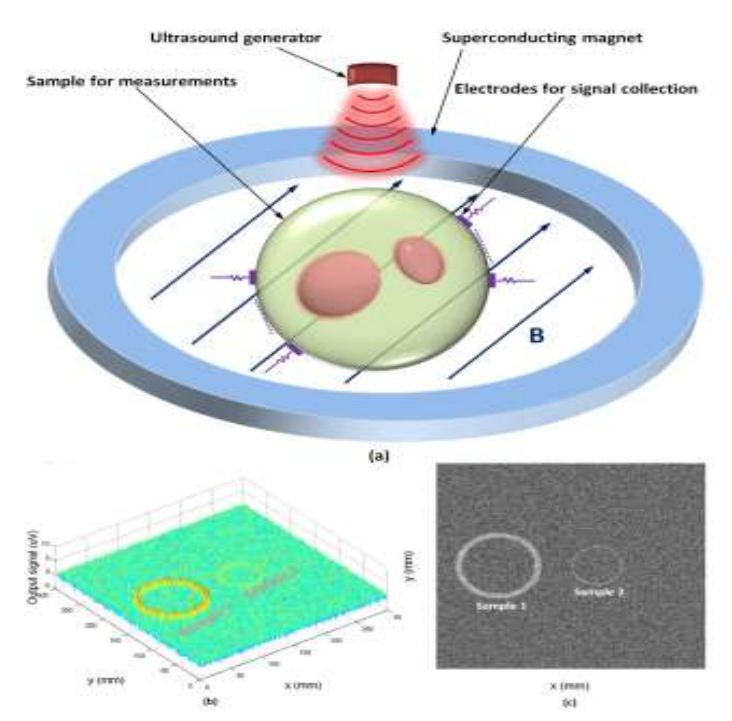


FIGURE 8: (a) Configuration of superconducting Lorentz Force Electrical Impedance Tomography (LFEIT), (b) magneto-acoustic signal from the superconducting LFEIT system, for the tests of two biological samples (output signal with noise), (c) electrical signal imaging of two biological samples, with figure source: [52].

Reference

[1] "Matthias, B. T.; Geballe, T. H.; Compton, V. B. Superconductivity. Rev. Mod. Phys. 1963, 35, 1–22.".

- [2] "Riedinger, R.; Wallucks, A.; Marinkovic, I.; Lo schnauer, C.; Aspelmeyer, M.; Hong, S.; Gröblacher, S. Remote Quantum Entanglement between Two Micromechanical Oscillators. Nature".
- [3] "Place, A. P. M.; Rodgers, L. V. H.; Mundada, P.; Smitham, B. M.; Fitzpatrick, M.; Leng, Z.; Premkumar, A.; Bryon, J.; Sussman, S.; Cheng, G. et al. A. New Material Platform for Superconducting Transmon Qubits with Coherence Times Exceeding 0.3 ms. 2020. a".
- [4] "Onnes, K. H. The Resistance of Pure Mercury at Helium Temperatures. Commun. Phys. Lab Univ Leiden B 1911, 12, 1.".
- [5] "Bardeen, J.; Cooper, L. N.; Schrieffer, J. R. Theory of Superconductivity. Phys. Rev. 1957, 108, 1175–1204.".
- [6] "A. Pawlak, Phys. J. 2014, 13, Heft 6, 6–7.".
- [7] "L. N. Cooper, Phys. Rev. 1956, 104, 1189–1190.".
- [8] "R. A. Shukor, High Temperature Superconductors: Materials, Mechanisms and Applications, Akademi Sains, Malaysia (2009).".
- [9] "A. Vilenkin and E. P. S. Shellard, Cosmic Strings and other Topological Defects, Cambridge University Press, Cambridge (1994).".
- [10] "J. R. Schrieffer: Theory of Superconductivity (Westview Press, Oxford, U.K, 1999).".
- [11] "C. Buzea, T. Yamashita, Supercond. Sci. Techn. 14 (2001) R115.".
- [12] "J. M. Tarascon, L. H. Greene, W. R. McKinnon, G. %. Hull, and T. H. Geballe, Science 235, 1373 (1987).".
- [13] "H. Maeda, Y. Tanaka, M. Fukutomi, and T. Asano, Jpn. J. Appl. Phys. Lett. 4, L209 (1988).".
- [14] "J. M. Tarascon, %. R. McKinnon, L. H. Greene, G. %. Hull, and E. M. Vogel, Phys. Rev. 8 36, 226 (1987)".
- [15] "Eisaki, H.; Kaneko, N.; Feng, D.L.; Damascelli, A.; Mang, P.K.; Shen, K.M.; Shen, Z.-X.; Greven, M. Effect of chemical inhomogeneity in bismuth-based copper oxide superconductors. Phys. Rev. B 2004, 69, 064512. [Google Scholar]".
- [16] "Gadermaier, C.; Kabanov, V.V.; Alexandrov, A.S.; Stojchevska, L.; Mertelj, T.; Manzoni, C.; Cerullo, G.; Zhigadlo, N.; Karpinski, J.; Cai, Y.Q.; et al. Strain-Induced Enhancement of the Electron Energy Relaxation in Strongly Correlated Superconductors. Ph".
- [17] "Norman, M.R. Entering the Nickel Age of Superconductivity. Physics 2020, 13, 85.".
- [18] "Orenstein, J.; Millis, A.J. Advances in the Physics of High-Temperature Superconductivity. Science 2000, 288, 468–474. [Google Scholar]".
- [19] "Presland, M.R.; Tallon, J.L. Superconductivity at 105 K in Tl0.5Pb0.5CaSr2-xLaxCu2O7. Phys. C 1991, 177, 1".
- [20] "no, A. High-Pressure Synthesis of Mo-Containing 1212 and 1222 Compounds, (Cu, Mo)Sr2YCu2Ozand (Cu, Mo)Sr2(Y, Ce)2Cu2Oz. Jpn. J. Appl. Phys. 1993, 32, 4517–4520. [Google Scholar]".
- [21] "Marezio, M.; Chmaissem, O.; Bougerol, C.; Karppinen, M.; Yamauchi, H.; Geballe, T.H. Overdoped cuprates with high-temperature superconducting transitions. APL Mater. 2013, 1, 021103.".
- [22] "Ono, A. Superconductivity in Cr-1212 cuprates Sr2-xBaxYCu2.8Cr0.2Oz. Jpn. J. Appl. Phys. Part 2 1995, 34, 1528. [Google Scholar]".
- [23] "Radaelli, P.G.; Perroux, M.; Marezio, M.; de Brion, S.; Tholence, J.L.; Huang, Q.; Santoro, A. Synthesis and Properties of a Cuprate Superconductor Containing Double Mercury-Oxygen Layers. Science 1994, 265, 380–383. [Google Scholar]".
- [24] "Yang, H.; Liu, Q.Q.; Li, F.Y.; Jin, C.Q.; Yu, R.C. Structure and microstructure of superconductor Sr2CuO3+δ (nominal delta=0.4) prepared under high pressure. Supercond. Sci. Technol. 2006, 19, 934.".

[25] "De Leon, J.M.; Conradson, S.D.; Batistić, I.; Bishop, A.R.; Raistrick, I.D.; Aronson, M.C.; Garzon, F.H. Axial oxygen-centered lattice instabilities in YBa2Cu3O7: An application of the analysis of extended x-ray-absorption fine structure in anharmonic sys".

- [26] "Lee, H.G.; Litvinchuk, A.P.; Abrashev, M.V.; Iliev, M.N.; Xu, S.H.; Chu, C.W. Raman spectroscopy of YSr2Cu3O7+δ. J. Phys. Chem. Solids 1998, 59, 1994. [Google Scholar]".
- [27] "Grigoraviciute, I.; Karppinen, M.; Chan, T.-S.; Liu, R.-S.; Chen, J.-M.; Chmaissem, O.; Yamauchi, H. Electronic Structures, Hole-Doping, and Superconductivity of the s = 1, 2, 3, and 4 Members of the (Cu,Mo)-12s2 Homologous Series of Superconductive Coppe".
- [28] "Gauzzi, A.; Klein, Y.; Nisula, M.; Karppinen, M.; Biswas, P.K.; Saadaoui, H.; Morenzoni, E.; Manuel, P.; Khalyavin, D.; Marezio, M.; et al. Bulk superconductivity at 84 K in the strongly overdoped regime of cuprates. Phys. Rev. B 2016, 94, 180509. [Google".
- [29] "Karppinen, M.; Yamauchi, H.; Morita, Y.; Kitabatake, M.; Motohashi, T.; Liu, R.S.; Lee, J.M.; Chen, J.M. Hole concentration in the three-CuO2-plane copper-oxide superconductor Cu-1223. J. Solid State Chem. 2004, 177, 1037.".
- [30] "Karppinen, M.; Yamauchi, H.; Morita, Y.; Kitabatake, M.; Motohashi, T.; Liu, R.S.; Lee, J.M.; Chen, J.M. Hole concentration in the three-CuO2-plane copper-oxide superconductor Cu-1223. J. Solid State Chem. 2004, 177, 1037. [Google Scholar]".
- [31] "Geballe, T.; Marezio, M. Enhanced superconductivity in Sr2CuO4–v. Phys. C Supercond. 2009, 469, 680–684. [Google Scholar] [CrossRef]".
- [32] "Rial, C.; Moran, E.; AlarioFranco, M.A.; Amador, U.; Andersen, N.H. Structure and superconductivity of room temperature chemically oxidized La2-xNdxCuO4+y (00≤x≥0.5). Phys. C 1997, 288, 91. [Google Scholar]".
- [33] "Matveev, A.; Ramirez-Castellanos, J.; Matsui, Y.; Takayama-Muromachi, E. New high-Tc superconductor, (GezCu1-z)Sr2Ca2-xYxCu3Oy ((Ge, Cu)-1223) prepared under high pressure. Phys. C Supercond. 1996, 262, 279–284.".
- [34] "H. W. Weijers, U. P. Trociewitz, W. D. Markiewicz, J. Jiang, D. Myers, E. E. Hellstrom, et al., 'High field magnets with HTS conductors', IEEE Trans. Appl. Supercond., vol. 20, no. 3, pp. 576-582, Jun. 2010.".
- [35] "L. Bortot, B. Auchmann, I. C. Garcia, H. D. Gersem, M. Maciejewski, M. Mentink, et al., 'A coupled A–H formulation for magneto-thermal transients in high-temperature superconducting magnets',".
- [36] "H. W. Weijers, H. Kandel, H. Bai, A. V. Gavrilin, Y. L. Viouchkov, D. C. Larbalestier, et al., 'Progress in the development of a superconducting 32 t magnet with REBCO high field coils', IEEE Trans. Appl. Supercond., vol. 24, no. 3, Jun. 2014.".
- [37] "C. Lorin and P. J. Masson, 'Numerical analysis of the impact of elliptical fields on magnetization losses', IEEE Trans. Appl. Supercond., vol. 23, no. 3, Jun. 2013.".
- [38] "B. Gamble, G. Snitchler and T. MacDonald, 'Full power test of a 36.5 MW HTS propulsion motor', IEEE Trans. Appl. Supercond., vol. 21, no. 3, pp. 1083-1088, Jun. 2011.".
- [39] "J. Geng, K. Matsuda, L. Fu, B. Shen, X. Zhang and T. A. Coombs, "Operational research on a high-textTtextrmc rectifier-type superconducting flux pump ", Supercond. Sci. Technol., vol. 29, no. 3, Mar. 2016.".
- [40] "Z. Huang, H. S. Ruiz, Y. Zhai, J. Geng, B. Shen and T. A. Coombs, 'Study of the pulsed field magnetization strategy for the superconducting rotor', IEEE Trans. Appl. Supercond., vol. 26, no. 4, Jun. 2016.".
- [41] "Z. Hong, A. M. Campbell and T. A. Coombs, 'Computer modeling of magnetisation in high temperature bulk superconductors', IEEE Trans. Appl. Supercond., vol. 17, no. 2, pp. 3761-3764, Jun. 2007.".
- [42] "Z. Hong, A. M. Campbell and T. A. Coombs, 'Numerical solution of critical state in superconductivity by finite element software', Supercond. Sci. Technol., vol. 19, no. 12, pp. 1246-1252, Dec. 2006.".

[43] "M. Zhang and T. Coombs, '3D modeling of high-Tc superconductors by finite element software', Supercond. Sci. Technol., vol. 25, no. 1, Dec. 2011.".

- [44] "M. Zhang, K. Matsuda and T. A. Coombs, 'New application of temperature-dependent modelling of high temperature superconductors: Quench propagation and pulse magnetization', J. Appl. Phys., vol. 112, no. 4, Aug. 2012.".
- [45] "M. Kapolka, V. Zermeno, S. Zou, A. Morandi, P. Ribani, E. Pardo, et al., 'Three-dimensional modeling of the magnetization of superconducting rectangular-based bulks and tape stacks', IEEE Trans. Appl. Supercond., vol. 28, no. 4, 2018.".
- [46] "M. D. Ainslie, H. Fujishiro, T. Ujiie, J. Zou, A. R. Dennis, Y.-H. Shi, et al., 'Modelling and comparison of trapped fields in (RE)BCO bulk superconductors for activation using pulsed field magnetization', Supercond. Sci. Technol., vol. 27, no. 6, Jun. 20".
- [47] "M. D. Ainslie, H. Fujishiro, H. Mochizuki, K. Takahashi, Y.-H. Shi, D. K. Namburi, et al., 'Enhanced trapped field performance of bulk high-temperature superconductors using split coil pulsed field magnetization with an iron yoke', Supercond. Sci. Technol".
- [48] "A. G. Page, A. Patel, A. Baskys, S. C. Hopkins, V. Kalitka, A. Molodyk, et al., 'The effect of stabilizer on the trapped field of stacks of superconducting tape magnetized by a pulsed field', Supercond. Sci. Technol., vol. 28, no. 8, Aug. 2015.".
- [49] "A. Baskys, A. Patel, S. Hopkins and B. Glowacki, 'Modeling of trapped fields by stacked (RE)BCO tape using angular transversal field dependency', IEEE Trans. Appl. Supercond., vol. 26, no. 3, Feb. 2016.".
- [50] "S. Zou, V. M. R. Zermeno and F. Grilli, 'Influence of parameters on the simulation of HTS bulks magnetized by pulsed field magnetization', IEEE Trans. Appl. Supercond., vol. 26, no. 4, Jun. 2016.".
- [51] "S. Zou, Magnetization of High Temperature Superconducting Trapped-Field Magnets, Karlsruhe, Germany:KIT Scientific, 2017.".
- [52] "B. Shen, L. Fu, J. Geng, X. Zhang, H. Zhang, Q. Dong, et al., 'Design and simulation of superconducting lorentz force electrical impedance tomography (LFEIT)', Phys. C Supercond., vol. 524, pp. 5-12, May 2016.".